Global climatological relationships between satellite biological and physical observations and upper ocean properties

Cara Wilson

Environmental Research Division, NOAA National Marine Fisheries Service Southwest Fisheries Science Center, Pacific Grove, California, USA

Victoria J. Coles

University of Maryland Center for Environmental Science, Horn Point Laboratory, Cambridge, Maryland, USA

[1]   We evaluate the relationships of monthly climatological satellite measurements of sea surface height, temperature and chlorophyll-*a* to climatological subsurface parameters (mixed layer depth, thermocline depth, and Z_{2N}, the 2 µmol NO_3 isocline depth) on a global scale to determine the spatial variability and mechanisms underlying their relationships. The goal is to situate satellite surface data in the context of subsurface processes so that ultimately surface variability on longer timescales can be related to physical processes. There are well-defined physical regimes in the tropics (20°S–20°N), where surface and subsurface physical parameters are predominantly positively correlated because of the dominance of baroclinic processes, and the extratropics (20°–60° latitude), where they are negatively correlated, and barotropic processes dominate. The biological regimes differ between these regions. Correlations between surface chlorophyll and subsurface parameters are variable in the tropics, positive at midlatitudes (20°–40° latitude) and negative at high latitudes. We interpret these changing relationships in the context of differing underlying biophysical processes: dynamic uplift causing nutrient entrainment into the euphotic zone in parts of the tropics, seasonal entrainment of nutrients into the euphotic zone at midlatitudes, and seasonal controls on light supply at high latitudes. Together with the physical regimes, these biophysical conceptual models explain the relatively complex, broad-scale relationships between global satellite measurements of sea surface height, temperature, and chlorophyll-*a* on a climatological seasonal basis.

Citation: Wilson, C., and V. J. Coles (2005), Global climatological relationships between satellite biological and physical observations and upper ocean properties, *J. Geophys. Res.*, *110*, C10001, doi:10.1029/2004JC002724.

1.   Introduction

[2]   Satellite data provide a unique perspective on natural and anthropogenic climate change on large scales, but determining the mechanisms underlying their observed variability will require a better understanding of the interactions between ocean-atmosphere coupling, ocean biology and CO_2 drawdown. Variability in both the mixed-layer depth (MLD, the surface zone of near-uniform temperature) and the thermocline depth (TD, the depth of maximum thermal gradient) are important to these processes because of their impacts on both surface biology and the air-sea CO_2 flux [*Ito and Follows*, 2003]. Currently, there is no established means of inferring subsurface density or biogeochemical structure directly from surface satellite data, although there has been some success reconstructing subsurface structure in regional areas using in situ data in conjunction with satellite data [*Carnes et al.*, 1994; *Chu et al.*, 1997; *Guinehut et al.*, 2004; *Nardelli and Santoleri*, 2004]. Knowledge of this subsurface thermal and salinity structure is also critical to assimilation of satellite data into predictive models [*De Mey*, 1997; *Han et al.*, 2004; *Ji et al.*, 2000; *Maes*, 1999]. Subsurface variability inferred from satellite data has been used to speculate on both the type of phytoplankton observed by satellite ocean color [*Coles et al.*, 2004; *Wilson*, 2003], and on interannual variability in production [*Carr et al.*, 2004]. This study seeks to better quantify the broad-scale spatial and temporal relationships between climatological satellite observations: sea surface height (SSH), sea surface temperature (SST) and upper ocean chlorophyll-*a* (CHL) and subsurface parameters (MLD and TD) to improve the mechanistic inferences that can be made from satellite data and to form a basis for the interpretation of variability in the satellite data.

[3]   SSH variability, in contrast to SST or CHL measurements, reflects an integrated measure of variability over the full depth of the water column. Once corrected for tidal and atmospheric pressure effects, the primary components in SSH variability are steric effects (density changes from heating, cooling or salinity changes) and wind forcing [*Fu*, 2001]. Heating and cooling of the upper ocean dominate seasonal SSH variability [*Gill and Niiler*, 1973], with

salinity changes important only in some regional areas [*Sato et al.*, 2000]. Whether the ocean responds baroclinically or barotropically to wind forcing varies on different spatial and temporal scales, but generally, the response is barotropic outside the tropics, and baroclinic within the tropics [*Fu*, 2001]. These responses partially dictate how SSH variability relates to the variability in TD. At the mesoscale, SSH variability mostly reflects changes in subsurface thermal or density structure, and consequently SSH anomalies are often used to infer the relative motion of the thermocline, and to estimate absolute changes in the surface layer depth using a baroclinic equation [*Siegel et al.*, 1999; *Tilburg et al.*, 2002]. The validity of this assumption has been tested in the tropics, where it appears to be a good approximation [*Pingree et al.*, 2002; *Rebert et al.*, 1985; *Ryan et al.*, 2002; *Turk et al.*, 2001]. Outside of the tropics, however, the correlation between SSH and TD is reduced by both a deeper and more diffuse thermocline, and by stronger surface buoyancy fluxes [*Mayer et al.*, 2001; *Rebert et al.*, 1985; *Stammer*, 1997]. Since temperature changes dominate fluctuations in surface density in most of the ocean, SST data can also be used to infer MLD or TD [*Chu et al.*, 2000; *Houghton*, 1991; *Nardelli and Santoleri*, 2004], although in regions subject to multiple forcings, such as the tropics, the relationship between surface parameters and subsurface structure becomes complicated [*Houghton*, 1991; *Mayer et al.*, 2001]. However, large-scale patterns in satellite fields suggests that satellite data may be useful in inferring subsurface structure [*Le Quéré et al.*, 2002; *Wilson and Adamec*, 2002].

[4] The ability to use satellite SSH and SST data to infer MLD and TD variability is important because variations in both MLD and TD influence upper ocean ecosystems. Both parameters can be thought of as defining the surface ocean layer, and generally, MLD and TD are assumed to vary synchronously, as a deepening MLD results in a deeper TD, and the seasonal thermocline tends to track the restratification associated with a shoaling MLD. However, the quantities are dynamically different. MLD is set by the depth of penetration of surface turbulence generated by wind and buoyancy forcing. TD responds to large-scale wind stress curl, as well as variability associated with seasonal restratification. As MLD increases, vertical entrainment brings nutrients toward the surface where light levels are higher, thereby enhancing biological production if the system is not light limited [*Bissett et al.*, 1994; *Gardner et al.*, 1999]. In past studies, the thermocline is often assumed to be correlated with the nutricline, with the corresponding inference that TD variations also shoal or deepen the nutricline, affecting the nutrient level of waters entrained into the mixed layer [e.g., *Herbland and Voituriez*, 1979; *Turk et al.*, 2001].

[5] A strong CHL-TD correlation would be expected where nutrients are limiting and the thermocline is close to the surface, such as in the tropics and in upwelling regions. Generally a good correlation between both CHL-SSH and CHL-TD has been observed in the tropical Pacific [*Chavez et al.*, 1998; *Turk et al.*, 2001; *Wilson and Adamec*, 2001; *Wilson and Adamec*, 2002]. However, over large regions of the global ocean the CHL-SSH relationship suggests that either the SSH-TD-nutrient flux paradigm is invalid, or that vertical nutrient fluxes are not the primary

control on surface biomass [*Wilson and Adamec*, 2002]. This observation is consistent with recent studies implicating the importance of lateral advection of nutrients to the productivity of the ocean gyres [*Jenkins and Doney*, 2003; *Oschlies*, 2002; *Williams and Follows*, 1998]. Of course, the physical controls on surface biomass associated with MLD or TD controls on light and nutrients cannot account for chlorophyll variability associated with grazing pressure, or aeolian deposition of micronutrients.

[6] Analyses of the relationship between surface observations (SSH, SST and CHL) and subsurface parameters (MLD and TD) have been confined mostly to localized areas where sufficiently long subsurface time series exist, and have been primarily in the tropical ocean [*Chu et al.*, 2000; *Guinehut et al.*, 2004; *Houghton*, 1991; *Nardelli and Santoleri*, 2004; *Pingree et al.*, 2002; *Rebert et al.*, 1985; *Ryan et al.*, 2002; *Turk et al.*, 2001]. Some larger-scale studies have inferred subsurface behavior from the differing geographical correlations between satellite SSH and CHL [*Le Quéré et al.*, 2002; *Wilson and Adamec*, 2002].

[7] Here we examine satellite data in conjunction with subsurface parameters on global spatial scales and climatological temporal scales to directly evaluate how they covary. Since insufficient subsurface data currently exist to look at interannual time series globally, we use monthly climatologies to investigate the seasonal relationships between satellite measurements of SSH, SST and CHL and the subsurface parameters of the MLD, TD and Z_{2N}, the 2 μmol mol NO_3 isocline depth. Our goal is to understand on broad spatial and temporal scales the relationship between the surface, observable quantities of SSH, SST, and CHL, and the subsurface properties that govern light and nutrient availability. While correlations between ocean properties that may be expected to have a seasonal cycle are not surprising, the spatial patterns in the correlation fields demonstrate different relationships among the variables that can be related to mechanistic hypotheses. Ultimately these large-scale relationships may be linked to factors that cause interannual variability on large spatial scales in phytoplankton production.

[8] Specifically, we examine four interrelated hypotheses: (1) MLD and TD covary, (2) SSH anomalies can be used at large spatial and temporal scales to infer the behavior of the depth of the surface ocean layer (MLD or TD), (3) the thermocline is a proxy for Z_{2N}, and (4) causal linkages between SSH anomalies and the Z_{2N} and MLD create a relationship between SSH and CHL.

2. Data and Methods

[9] Satellite data from 1999 to 2003 were used to make global 1° monthly climatologies of SSH, SST, and CHL. Data from 1997 to 1998 were excluded to avoid aliasing from the strong ENSO event during that period. The merged SSH product, using data from TOPEX/Poseidon and the ERS satellites, was obtained from Archiving, Validation, and Interpretation of Satellite Oceanographic (AVISO) (http://www.aviso.oceanobs.com/). Reynolds SST analysis was used [*Reynolds et al.*, 2002], and Sea-viewing Wide Field-of-view Sensor (SeaWiFS) chlorophyll-*a* data were obtained from the NASA Goddard Space Flight Center Distributed Active Archive Center (DAAC) (http://
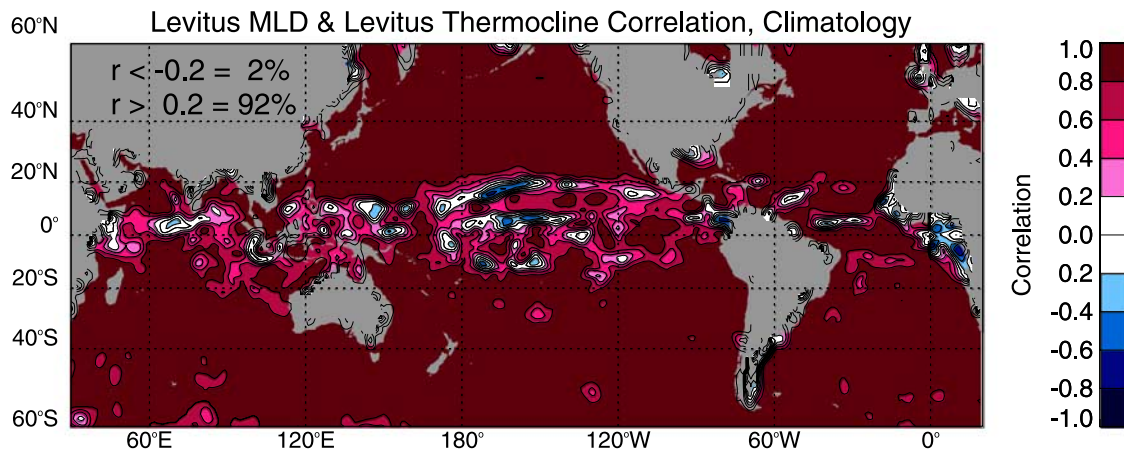
Figure 1. Correlation between monthly climatological values of mixed layer depth (MLD) and thermocline depth (TD). Absolute correlations >0.4 are significant at the 80% confidence level. Contour interval is 0.2.

daac.gsfc.nasa.gov). MLD fields and temperature profiles were obtained from the Levitus data set [*Levitus and Boyer*, 1994] distributed by the Climate Data Library at Columbia University's Lamont-Doherty Earth Observatory (http://ingrid.ldgo.columbia.edu). The Levitus MLD data are calculated using a density criterion of 1.25×10^{-4} kg m^{-3}. The analyses were also performed using MLD climatologies produced by the Naval Research Laboratory [*Kara et al.*, 2003] and the Laboratoire d'Océanographie Dynamique et de Climatologie [*de Boyer Montégut et al.*, 2004] (not shown). There are only minor differences in the results using the other MLD fields, and they do not affect the overall large-scale patterns presented here. We have chosen to remain with the Levitus MLD to maintain spatial consistency with the TD calculation.

[10] The TD is calculated as the shallowest local maximum in the vertical temperature gradient below the MLD. This definition is used instead of the depth of the maximum temperature gradient in order to distinguish the seasonal thermocline from the deeper permanent thermocline. The seasonal thermocline is used here because it reflects the depth of vertical mixing, and so is the biologically relevant choice. The determination of a globally consistent TD is a challenge. Criteria such as the maximum vertical temperature gradient, thresholds of vertical gradient, and latitudinally varying isopycnal depths failed to yield consistent results based on visual inspection of the thermocline depth plotted against vertical sections of temperature.

[11] The monthly objectively analyzed nitrate values from the World Ocean Atlas 2001 database [*Conkright et al.*, 2002] are used to calculate Z_{2N}, the depth of the 2 μmol NO_3 isocline. The vertical gradient in nutrient is less relevant to CHL than the absolute concentration available for uptake by plankton. Thus, although the nutricline gradient governs local diffusion of nutrients, we are invoking seasonal entrainment into the mixed layer as the dominant nutrient flux mechanism, which is independent of the vertical gradient in nutrient concentration. This definition also reduces the errors associated with determining the vertical gradient in a noisy field.

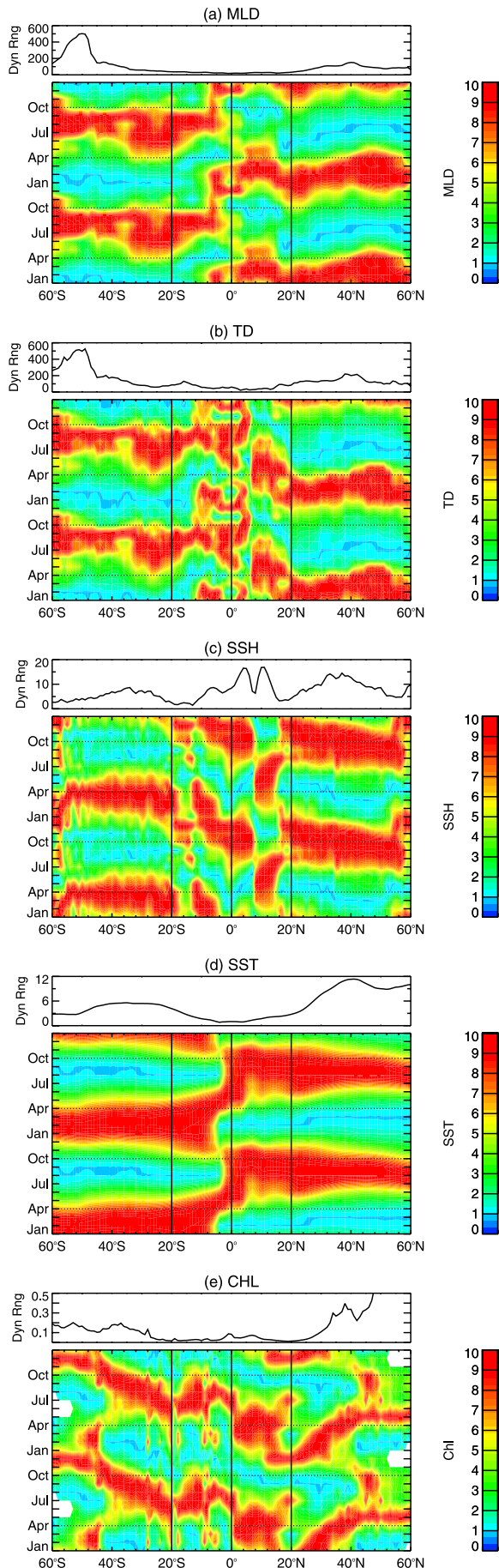[12] All surface and subsurface fields are smoothed with a 5° spatial running box mean, and a three month temporal running box mean before analysis. Correlation maps shown below are further postfiltered with a 3° spatial running box mean. Different scales, and anisotropic smoothing were performed, none of which altered the large-scale patterns. The smoothing reduces small-scale variability, better emphasizing the large-scale patterns of interest.

3. Results

3.1. Surface Layer (MLD and TD)

[13] The boundary between the surface layer and deep water in a conceptual two-layer ocean can be defined as either the MLD or the TD, depending on whether the distinction is dynamical or biological. Here we look at both parameters as indicators of the depth of the surface layer, and compare them to variability observed in satellite data. Often, MLD and TD have been assumed to vary synchronously, as a deepening MLD results in a deeper TD, and the seasonal thermocline tends to track the restratification associated with a shoaling MLD.

[14] To examine the hypothesis that the MLD and the TD covary, global correlations between them are shown in Figure 1. While correlations do not imply causality, they indicate the degree to which variables are in (or out of) phase, which can be used to understand the underlying dynamics affecting them, particularly where mechanistic interactions linking the processes are identified. As expected, the MLD and TD are positively correlated (R > 0.8) throughout most of the global ocean. However, within the tropics (20°S–20°N), there are regions of weaker positive correlations, as well as some areas of negative correlations. This might be expected, as the annual cycles in heating and mechanical stirring are less coupled, and individually weaker, in the tropics. A disconnect between TD and MLD variability on seasonal (but not on interannual) timescales has also been observed in in situ measurements from the equatorial Pacific [*Cronin and Kessler*, 2002]. The regions of negative, or weakly positive correlations, generally fall along three zonal bands in the Atlantic and Pacific: 10°S, 5°N and 15–20°N, with maxima away from the western boundaries in the central ocean basins. To better understand the MLD-TD correlations, a repeating

seasonal cycle is plotted for the zonally averaged MLD and TD in Figures 2a and 2b. The dynamic range for both MLD and TD is seen to be low in the tropics, particularly for MLD, which tends to weaken the correlation between the two. While the seasonal cycles in both parameters shift between the tropics and the extratropics, there are some significant differences in their seasonal transitions. Both have a summer maximum and winter minimum outside of the tropics, but the changes from Southern to Northern Hemisphere dynamics occur at different latitudes.

[15] The northernmost band of disconnect between TD and MLD occurs at 15–20°N. As seen in Figures 2a and 2b, there is a transition in the seasonal cycle at these latitudes, from a December-March maximum in both properties north of 15°N to a maximum 2–3 month later closer to the equator. While this transition occurs abruptly in the MLD, preceded by a slightly earlier winter MLD maximum, it occurs more gradually in the TD, and between 18–20°N, there is a semiannual signal, with a TD minimum in March separating the two maxima. Thus the weakened MLD-TD correlation here is probably caused by the secondary TD maxima in January-February, which does not occur for the MLD. Colocated with this TD minimum is a local minimum in wind stress (from National Centers for Environmental Prediction Reanalysis, not shown), which may be driving the TD variability.

[16] The second band of decorrelation between MLD and TD occurs near 5°N and is associated with the Intertropical Convergence Zone (ITCZ). Both MLD and TD acquire a semiannual maximum near 5°N. MLD, however, transitions a few degrees closer to the equator than TD, and the winter-spring MLD maximum is greater than the summer-fall maximum, and the opposite is true for TD. The southern limit of these semiannual signals in MLD and TD occurs at 10°S, the third region of decorrelation, and is again associated with somewhat poleward transition in TD relative to the MLD transition.

[17] Differences between the seasonal dynamics of MLD and TD arise from the similar but different physical mechanisms that modulate them: wind speed and buoyancy forcing for MLD, and these, plus interactions with wind stress curl, for TD. The seasonality of the MLD, with its abrupt change in the month of the seasonal maximum near 8°S, is virtually identical to the seasonal pattern in wind speed (not shown). TD dynamics are more complicated, as the TD is affected by seasonal changes in both the sign and magnitude of the local wind stress curl, as well as through remote forcing by waves. Regions where the TD seasonality changes also coincide with regions with seasonal changes in the sign of the curl (not shown). However, the TD is also affected by the wind speed, for example, the local TD minimum in March at 20°N is preceded by a February minimum in wind speed at the same location (not shown).

Figure 2. Hovmöller diagrams showing the seasonal cycle averaged across the Pacific (145°E–120°W) of (a) MLD, (b) TD, (c) SSH, (d) SST and (e) CHL. The data have been normalized by the local dynamic range, which is shown above each figure. Two seasonal cycles are displayed. For reference, lines are drawn at 20°S, the equator, and 20°N, as well as in April and October.

[18] There are also some regions of negative correlations in the western Pacific near the warm pool, and in the Indian Ocean, that do not fall along obvious zonal bands. The negative correlations could result from the barrier layers that are found in these regions [*Sprintall and Tomczak*, 1992]. Barrier layers form where salinity gradients rather than thermal gradients dictate the depth of vertical mixing between the surface isohaline and isothermal layers. This layer increases surface stratification and restricts vertical mixing [*Lukas and Lindstrom*, 1991]. Seasonal formation of barrier layers will impact the MLD without influencing the TD, leading to a disconnect between MLD and TD variability.

[19] However, over much of the global oceans, MLD and TD covary strongly, indicating a similar seasonality in the factors that control them, and confirming our first hypothesis. In general, this relationship is weaker in the tropics, though even there, the negative or insignificant correlations occur in localized bands. Throughout the following discussion we will focus on the TD, with some exceptions related to the regions where MLD and TD do not covary.

3.2. Satellite Measurements and Surface Layer Thickness

[20] It is has often been assumed that our second hypothesis is correct; that positive SSH anomalies indicate a deeper thermocline [*Cipollini et al.*, 2000; *Garzoli and Goni*, 2000; *McClain et al.*, 2004; *Siegel et al.*, 1999; *Tilburg et al.*, 2002], and this can be clearly seen in the spatial pattern of mean SSH which shows the large-scale wind driven gyre circulations, as well as in mesoscale eddies SSH and TD structure, however, this has been tested only at limited temporal and spatial scales. This hypothesis implies a positive correlation between SSH and TD, since both quantities are defined here as layer thicknesses, rather than absolute depth referenced to a fixed vertical level. While the positive SSH/TD correlation is generally robust at the eddy scale [*Siegel et al.*, 1999; *Tilburg et al.*, 2002], or within the tropics [*Rebert et al.*, 1985; *Ryan et al.*, 2002; *Turk et al.*, 2001] our goal here is to evaluate its consistency on basin and global scales.

[21] To examine the geographic robustness of this relationship, correlations between surface (SSH and SST) and subsurface (TD and MLD) fields are shown in Figure 3. The expected positive correlations between SSH-TD and SSH-MLD are confined mainly to the tropics (20°S–20°N), with negative correlations elsewhere. Clearly, on annual timescales and large spatial scales, SSH should not be used as a proxy for TD or MLD. Significant variations exist even within this broad-scale pattern of positive tropical correlations. For example, the regions of positive correlations are smaller in the southern tropics than the northern tropics (particularly in the Atlantic and Indian oceans). This may relate to a hemispheric asymmetry in the large-scale gyre structures, as the Southern Hemisphere lacks a tropical gyre, and the subtropical gyre penetrates farther equatorward at the surface.

[22] The switch from positive to negative correlations occurs quite sharply at roughly 20° latitude, although it is slightly less abrupt in the south then in the north. This transition is caused by the change in SSH seasonality between 10° and 20° latitude, seen in Figure 2c, which is also less pronounced in the Southern Hemisphere. Several dynamics change across this 20°N and S transition. In the tropics wind-driven processes dominate SSH variability, while outside the tropics the steric effects associated with seasonal cooling and heating dominate [*Ferry et al.*, 2000; *Fukumori et al.*, 1998; *Mayer et al.*, 2001; *Stammer*, 1997]. In the extratropics as surface water warms in the summer the MLD and TD shoal. Relative to winter conditions, there is more warm, light water above a relatively shallow seasonal thermocline, leading to positive SSH anomalies, and negative SSH-TD correlations. The 20°N and S transition is also a separation point between the dominance of baroclinic processes in the tropics and barotropic processes elsewhere [*Chao and Fu*, 1995; *Fukumori et al.*, 1998]. A positive SSH/TD correlation represents baroclinic processes; with barotropic processes the sea surface and depth of the surface layer move in unison, resulting in a negative correlation (since SSH increases while TD is thinning or decreasing). The dominance of barotropic processes outside of the tropics is important, as it means that the baroclinic equation which was developed for, and has been used successfully for, equating mesoscale SSH anomalies to absolute changes in the TD [i.e., *Siegel et al.*, 1999; *Tilburg et al.*, 2002] is not applicable on large spatial scales outside of the tropics.

[23] Correlations between SST-TD and SST-MLD are shown in Figures 3c and 3d. With seasonal cooling, SST decreases and the MLD and TD deepen, resulting in a predominantly negative correlation throughout the global ocean. The negative relationship between SST and MLD (Figure 3d) is the most consistent globally, with only 3% of the ocean having significant positive correlations. This robust relationship reflects the interactions between both cooling and the MLD, and entrainment of deeper colder water and the MLD, which both act to maintain a negative SST-MLD correlation. The positive correlations along the equator result from a small latitudinal shift in the seasonal switch between the northern and southern hemisphere as discussed above. As seen in Figure 2d, the SST transition occurs just south of the equator (although there is meridional variation, the transition occurs slightly north of the equator on the eastern sides of the basins, not shown), but both the TD and MLD transition further off the equator (6°N and 8°S respectively), leading to positive correlations along the equator. There are additional regions of positive SST-TD correlations (Figure 3c) not echoed in the SST-MLD correlation map (Figure 3d) that are primarily associated with changes in the TD seasonality from migration of the ITCZ. These regions of positive correlations also have negative MLD-TD correlations (Figure 1), reflecting differences between the seasonal dynamics that drive the vertical migration of the thermocline, and the wind speed magnitude, which modulates the depth of mixing and the SST.

3.3. Thermocline and Nutricline

[24] Biologically, the thermocline is not of interest because of the effect of the maximum vertical temperature gradient on ecosystems, but rather because the thermocline is often used as a proxy for Z_{2N}. Assuming a tight relationship between the TD and Z_{2N}, changes in the depth of the thermocline will impact the vertical flux of nutrients to the surface, stimulating or suppressing surface biological production. To assess how well the TD represents the Z_{2N},
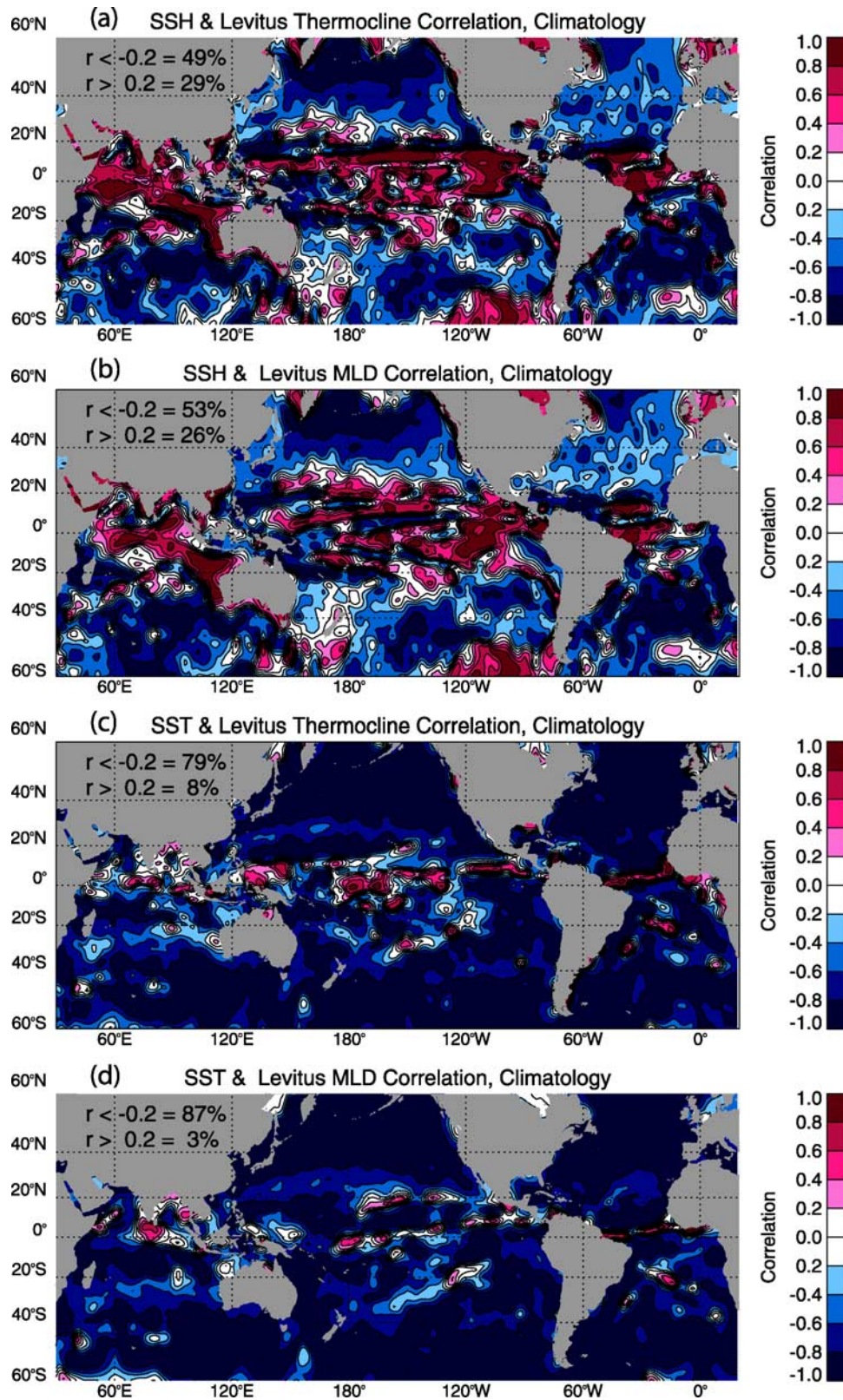
Figure 3. Maps of the correlation between monthly climatological values of (a) SSH and TD, (b) SSH and MLD, (c) SST and TD, and (d) SST and MLD. Absolute correlations >0.4 are significant at the 80% confidence level. Contour interval is 0.2.
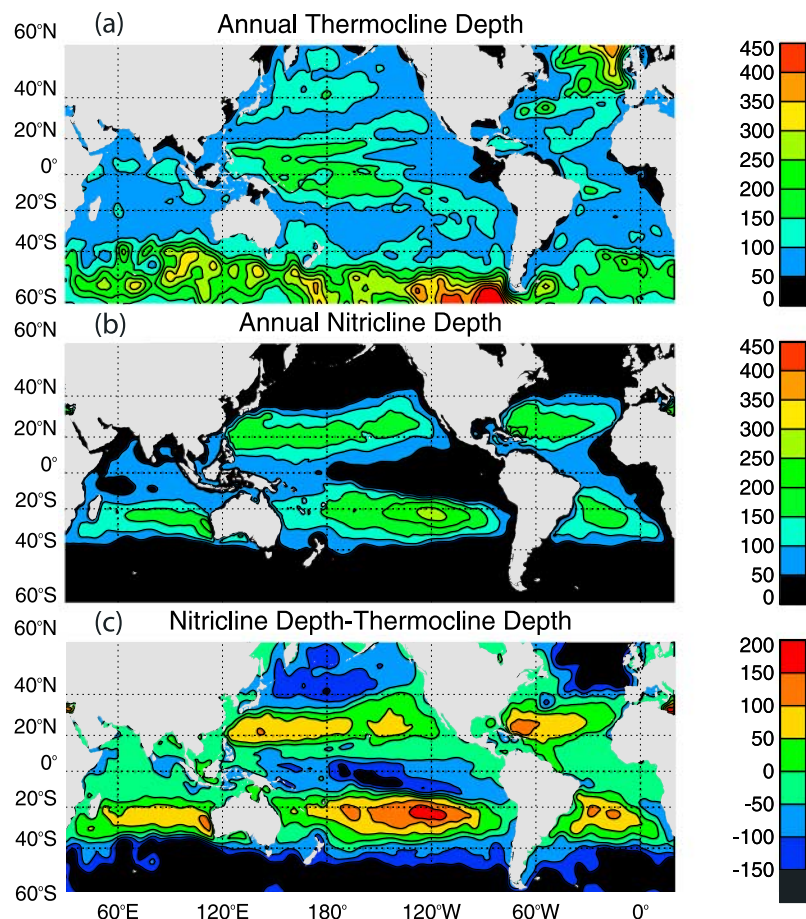
Figure 4. Annual depth of (a) thermocline, (b) Z_{2N} and (c) the difference between them. Negative (positive) values in Figure 4c indicate where Z_{2N} is above (below) the thermocline. Contour interval is 50 m.

the depth of the mean annual thermocline, Z_{2N}, and their difference are shown in Figure 4. On short timescales (seasonal) nitrate is assumed to be the limiting nutrient [*Lewis et al.*, 1986] outside of high-nutrient, low-chlorophyll (HNLC) regions, however phosphate limitation can also occur, particularly on longer timescales [*Cullen*, 1999; *Karl et al.*, 1997; *Tyrrell*, 1999]. Here NO_3 is used, however the resulting geographical patterns would be similar if PO_4 had been used. Throughout the tropical Atlantic and Indian Oceans, there is generally a good agreement between the Z_{2N} and thermocline, with their depths being within 50 m of one another (the green regions in Figure 4c), consistent with previous work [*Herbland and Voituriez*, 1979]. In the middle of the subtropical gyres, however, the Z_{2N} can be as much as 100–200 m deeper than the thermocline, resulting in the oligotrophic open ocean gyres. The deep Z_{2N} affects the availability of nutrients for supporting biological production, and these regions are also characterized by the lowest mean CHL values [*McClain et al.*, 2004].

[25] In HNLC regions, (high latitudes and most of the equatorial Pacific), Z_{2N} is at the surface (indicated by black in Figure 4b). In these areas production may be limited by iron [*Martin et al.*, 1990] or other micronutrients, and/or, on a seasonal basis, by light in the high latitudes. Iron-limited ecosystems should be less influenced by thermocline (Z_{2N})

changes; as the primary source of iron to the euphotic zone is atmospheric deposition [*Duce and Tindale*, 1991]. However, light-limited ecosystems will be impacted by MLD changes, with increased production occurring when shallow mixed layers trap phytoplankton in the photic zone.

3.4. Subsurface Variability and Chlorophyll

[26] Relationships between satellite-derived chlorophyll and the subsurface parameters are shown in Figure 5 and delineate three geographical regions: negative correlations in the subpolar regions (40°–60°), positive in the midlatitudes (20°–40°), and highly regionally variable in the tropics (20°S–20°N). Conceptual schematics illustrating the factors influencing the different regional ecosystem dynamics are shown in Figure 6. Time series of MLD, TD, Z_{2N}, CHL, SST, and SSH averaged over regions best illustrating these conceptual models are shown in Figure 7 to highlight the evolution of these quantities over the seasonal cycle.

[27] Different scenarios involving nutrient or light limitation can lead to positive or negative CHL/TD relationships as illustrated in Figure 6. Assuming a nutrient-limited system (Figure 6a), when the thermocline (nutricline) is lifted (as in upwelling), nutrients are brought into the surface layer, increasing chlorophyll, and resulting in a
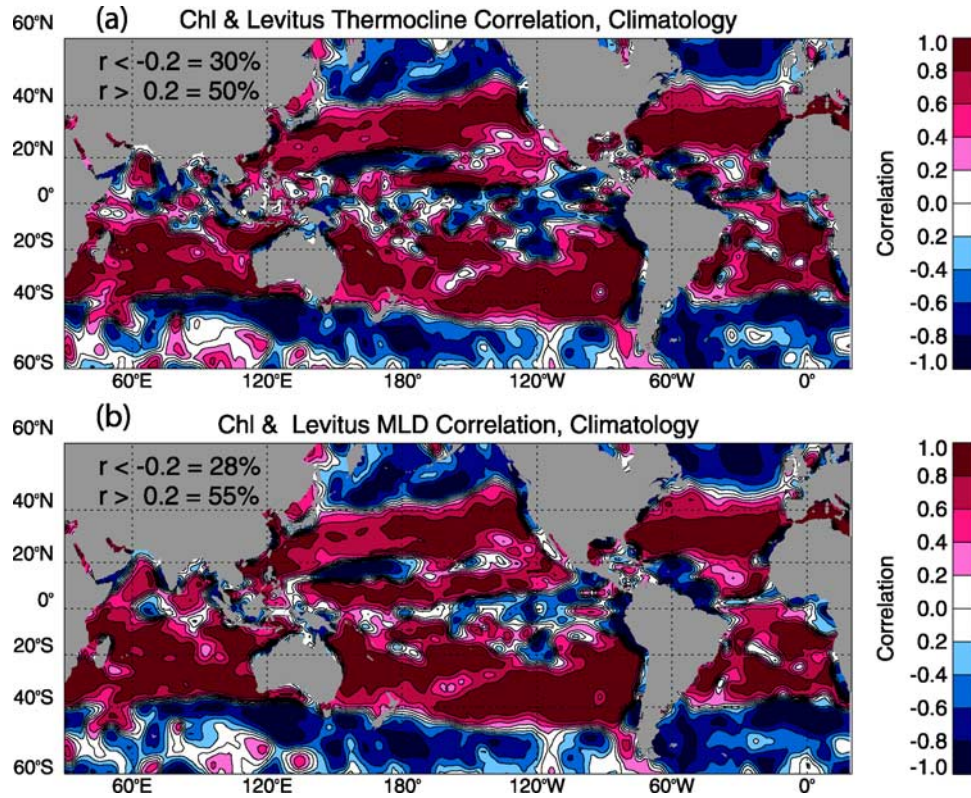
Figure 5. Correlations between monthly climatological values of (a) CHL and TD and (b) CHL and MLD. Absolute correlations >0.4 are significant at the 80% confidence level. Contour interval is 0.2.

negative CHL-TD relationship. This case corresponds to the regions of negative correlation between CHL and MLD/TD observed in the tropics. In the subtropics (Figure 6b), if the seasonal TD stratifies above the Z_{2N}, then nutrients will be limiting in the warm season, and winter mixing will deepen the seasonal TD and allow for entrainment of deep nutrients into the surface, increasing chlorophyll, and resulting in a positive CHL-TD relationship. In a light-limited system (Figure 6c), winter mixing creates high nutrient concentrations in the upper ocean, which cannot be utilized until springtime shoaling of the MLD traps phytoplankton within the surface euphotic zone, increasing chlorophyll, and resulting in a negative CHL-TD relationship. These different dynamics are discussed in more detail below in the context of the observed geographical relationships.

3.4.1. Tropics (20°S – 20°N)

[28] The tropics are characterized by variable correlations between CHL and the surface layer depth, with areas of both positive and negative correlations. Negative correlations correspond conceptually to the upwelling scenario (Figure 6a). In this case, a shallower TD brings more nutrients to the surface, increasing CHL and leading to negative CHL-TD correlations. Strong negative correlations consistent with upwelling regimes occur in the central equatorial Pacific and along the eastern boundary currents (Figure 5a). This pattern is illustrated in Figure 7a, where time series of MLD, TD, Z_{2N}, CHL, SST, and SSH are shown averaged over an upwelling region off of South America. Coincident with the uplift of the thermocline in January–March, the chlorophyll has its seasonal maximum.
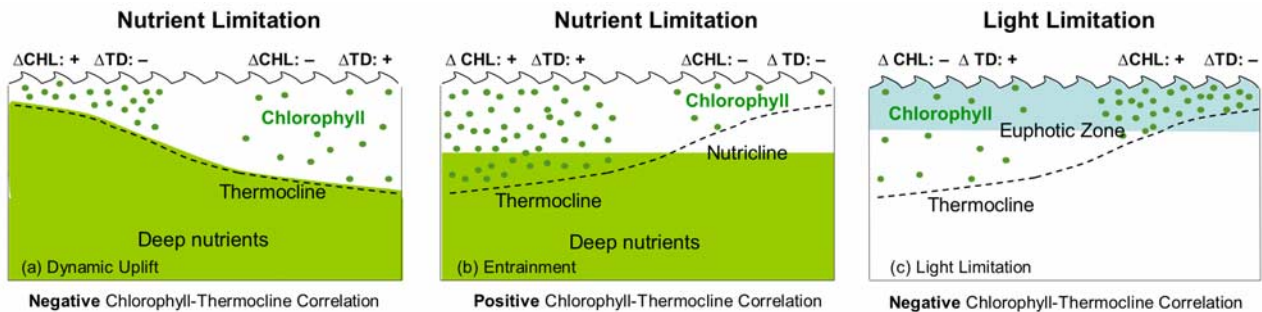

Figure 6. Schematics illustrating three scenarios for thermocline, Z_{2N}, euphotic depth, and chlorophyll interactions. (a) Dynamic uplift, (b) entrainment and (c) light limitation.
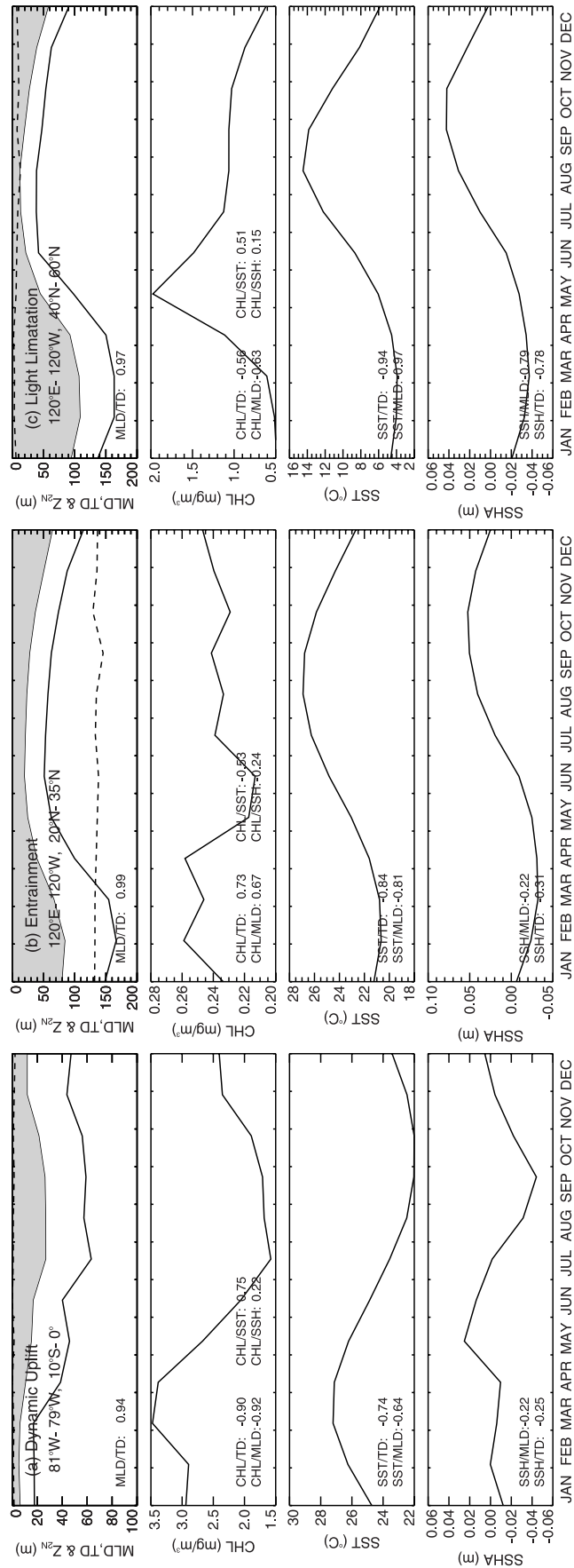
Figure 7. Seasonal cycles of subsurface and satellite fields averaged over different regions illustrating the three schematics shown in Figure 6. (a) Dynamic uplift (81°–79°W, 10°S–equator), (b) entrainment (120°E–120°W, 20°N–35°N), and (c) light limitation (120°E–120°W, 40°N–60°N). The first panel shows the mixed layer (shaded), Z_{2N} (dashed line) and the TD (solid line), second to fourth panels show CHL, SST, and SSH, respectively. Note that the vertical axes vary in the different regions.
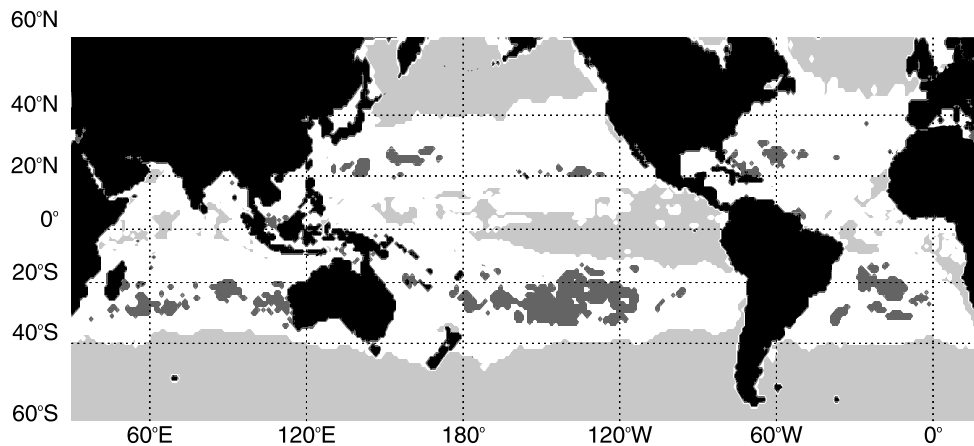
Figure 8. Seasonally varying relationship between the TD and Z_{2N}. Regions where the TD and Z_{2N} intersect at a period in their seasonal cycles (i.e., where the thermocline and Z_{2N} are seasonally decoupled) are white. In light gray regions the thermocline is always below Z_{2N}; in dark gray regions the thermocline is above Z_{2N} throughout the year.

[29] Parts of the tropics are iron-limited HNLC regions (see black shaded regions in Figure 4b) where variations in micronutrient supply will have a bigger impact on biological production than changes in the physical dynamics of the ocean. Although a causal relationship between CHL and TD would not be expected, even in these regions, the correlations tend to be negative. Positive correlations in the tropics occur in warm pool regions, in the central tropical gyres, and areas where the Z_{2N} is shallow enough throughout the year that increased MLD enhances nutrient supply, i.e., where the subtropical scenario in Figure 6b applies. This dynamic can be seen in Figure 7b. Although in this region the MLD does not intersect the Z_{2N} they are closest in the winter when CHL is at a maximum.

3.4.2. Midlatitudes (20°–40°)

[30] The midlatitudes are characterized by strong, positive correlations between CHL and MLD/TD, consistent with wintertime entrainment of the nutricline into the mixed layer (Figure 6b). However, as mentioned above, the upwelling scenario (negative correlation) is also evident along the eastern boundary of the Atlantic and Pacific in coastal upwelling regimes. To a first order, the entrainment scenario seems inconsistent with the broad regions of positive correlation because they are areas with the deepest Z_{2N}, which can be well below the thermocline (Figure 4). However, the correlations reflect only how well the parameters vary together, and the absolute values of the parameters must be taken into consideration to understand the underlying dynamics. The midlatitudes are the most oligotrophic parts of the ocean [*McClain et al.*, 2004], never experiencing high levels of biomass, as illustrated by the low dynamic range in Figure 2e. While there is not very much NO_3 above Z_{2N}, the small seasonal chlorophyll maximum in these regions does not require a large nutrient supply. The key distinction between the upwelling and entrainment scenarios in Figure 6 is the relationship between TD and Z_{2N}, and in regions with a positive CHL/TD (i.e., the midlatitudes), the thermocline and Z_{2N} should be seasonally decoupled from one another, with the permanent thermocline being associated with the Z_{2N}, and the seasonal thermocline restratifying above Z_{2N}. This does in fact occur, as seen in the seasonal cycles in Figure 7c, where at midlatitudes the MLD and TD deepen below Z_{2N} in winter, but are shallower or colocated the rest of the year. To see the geographical extent of this dynamic a map of the seasonally varying relationship between the TD and Z_{2N} is shown in Figure 8. Regions where TD and Z_{2N} intersect within a seasonal cycle (such as in Figure 7c) are in white; the shaded regions indicate coupled behavior where the two never intersect. Throughout most of the midlatitudes, Z_{2N} and thermocline movements are decoupled seasonally (white regions), consistent with the entrainment model. Exceptions to this occur in the dark gray regions of Figure 8, where Z_{2N} is always deeper than the thermocline (see Figure 4c). However, the behavior of Z_{2N} and the thermocline is the same in these regions, in that the depths of the two converge as the thermocline deepens in winter while Z_{2N} stays fixed. It should be noted that while the entrainment model requires TD and Z_{2N} movements to be seasonally uncoupled, their intersection does not necessarily imply that entrainment dynamics drive CHL. For example, in the equatorial regions where the TD and Z_{2N} are close to one another slight deviations in either of them could cause their intersection without fundamentally changing the dynamics. In addition, in light-limited regions, seasonal drawdown of nutrients can deepen the nutricline into the thermocline.

[31] The entrainment scenario would also apply when chlorophyll from the deep chlorophyll maximum (DCM) is entrained into the surface by a deeper MLD, although in this case the CHL increase would not be a result of new production. This dynamic has been observed in parts of the oligotrophic Pacific where wintertime mixing does not reach the nutricline [*McGowan and Hayward*, 1978; *Venrick*, 1993]. Either scenario, entrainment of nutrients or of the DCM, invokes a causal mechanism to explain the positive CHL-TD correlations. An additional, noncausal, explanation for the observed relationship would be a photoadaptive chlorophyll increase during the winter [*Letelier et al.*, 1993], which is coincident with, but independent of, changes in the MLD or TD.
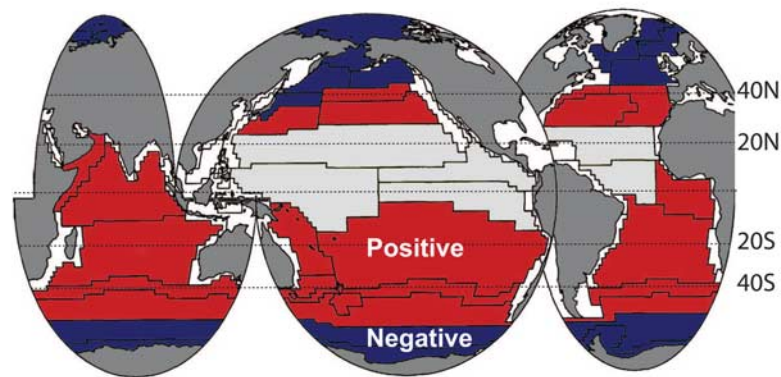
Figure 9. Open ocean biogeochemical provinces adapted from *Longhurst* [1995, 1998]. Regions where his model indicates negative (positive) CHL/TD correlations are in blue (red). Light gray regions correspond to where his model predicts little correspondence between physical and biological forcing.

3.4.3. Subpolar (40°–60°)

[32] The subpolar regions are characterized by negative CHL-TD correlations (Figure 5); however, the cause is consistent with the light limitation scenario (Figure 6c) rather than the upwelling scenario (Figure 6a). The change from negative to positive correlations near 40° latitude coincides with the surfacing of the ND (Figure 4b) leading to a larger nutrient flux for biological production. However, seasonal light limitation, due to the very deep winter mixed layers (Figure 2a) at these high latitudes, prevents phytoplankton growth during the winter nutrient injection. Phytoplankton growth is delayed until the MLD shoals in the spring. Figure 7c illustrates this seasonal cycle with data from the central Pacific subpolar gyre. MLD and TD are closely correlated, with Z_{2N} remaining at the surface throughout the year. SST and SSH are maximum in late summer/early fall due to heating and steric effects. The CHL response occurs in the spring, anticorrelated with MLD/TD, SSH, and SST, however, the anticorrelation is low because the CHL response is particularly abrupt and short-lived relative to the variability in MLD, TD, and SSH.

3.5. Biogeographical Provinces

[33] The three broad types of climatological seasonal biophysical interactions delineated here are consistent with results from biogeographical studies. *Longhurst* [1995, 1998] used climatological CZCS satellite chlorophyll data to partition the oceans into different ecological provinces and biomes. He developed five general models to describe biophysical dynamics in the open ocean: polar light limitation, midlatitude nutrient limitation, subtropical nutrient limitation, tropics with weak seasonality and monsoon dominated. His polar light-limiting model corresponds to the light limitation scenario (Figure 6c), his midlatitude, nutrient-limiting model corresponds to the upwelling scenario (Figure 6a), his subtropical and monsoon models to the entrainment scenario (Figure 6b), while his tropical model is characterized by no significant seasonal change in either biological or physical parameters. For each model he presented schematics of the seasonal cycles of chlorophyll and MLD [*Longhurst*, 1995]. Shown in Figure 9 are the open ocean provinces he defined, classified here by the seasonal relationship between CHL and MLD in their associated models – either positive, negative or a lack of correlation. The same general pattern that he defined previously is seen in Figure 5; negative correlations at high latitudes and positive ones throughout the midlatitudes. However, whereas our analysis shows significant, yet variable, correlations within the tropics, his model indicated little correspondence between CHL and MLD variability in
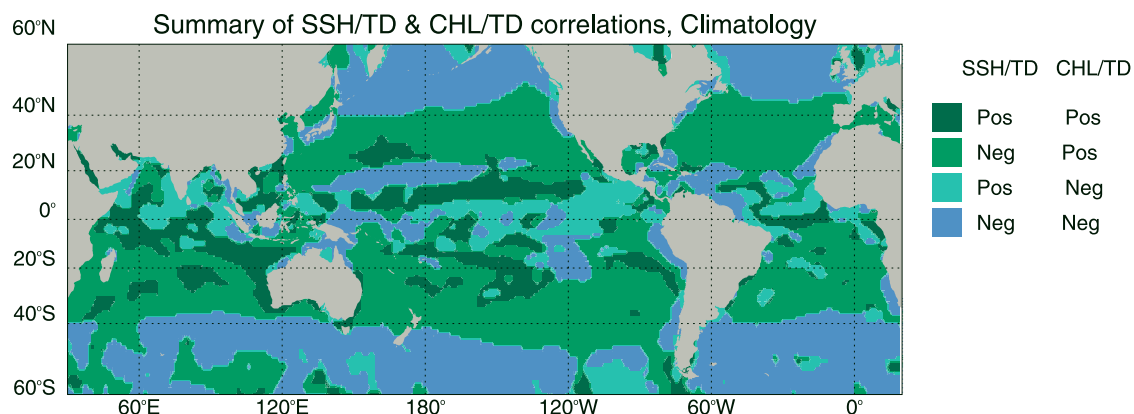

Figure 10. Schematic summary of the observed seasonal climatological relationships between SSH-TD and CHL-TD.
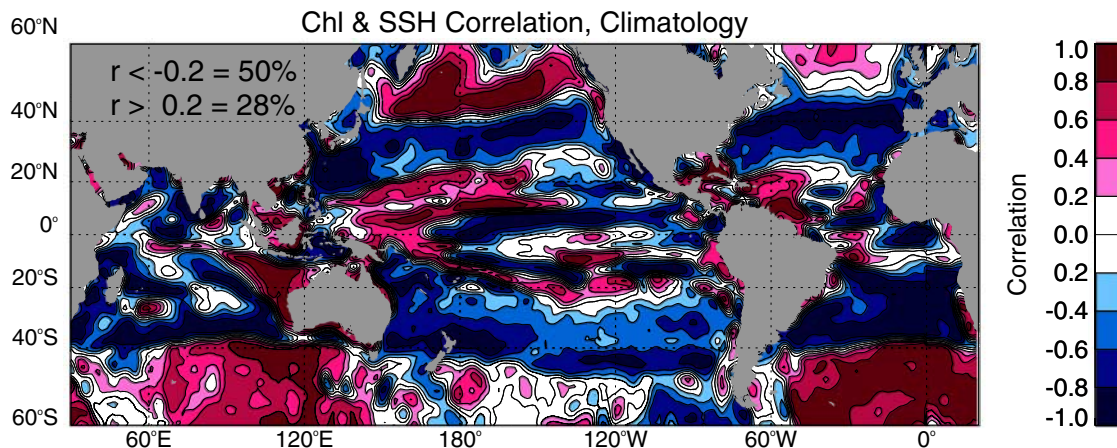
Figure 11. Correlations between SSH and CHL, both of which can be observed from space. Absolute correlations >0.4 are significant at the 80% confidence level. Contour interval is 0.2.

the tropics. Our results indicate that the boundary in the Southern Hemisphere between light and nutrient limitation occurs at 40°S, whereas his work has this transition further south near 50°S, and his northern tropical boundary at 30°N is further north than ours at 20°N.

4. Conclusions

[34] In summary we will revisit the hypotheses that were examined:

[35] 1. At the temporal and spatial scales of our analyses the MLD and TD (defined as the seasonal thermocline) generally covary throughout the oceans, except for some well-defined transitional regions at 20°N, 7°N, and 10°S, so the variability in MLD and TD is well represented with either property.

[36] 2. Relationships between the surface layer and satellite measurements (SSH and SST) have significant geographic variability. SSH has a broadly positive relationship with MLD/TD in the tropics, consistent with baroclinic dynamics. Negative correlations between SSH and MLD/TD occur outside the tropics due to steric processes. SST and MLD/TD are better correlated than SSH and MLD/TD, though this relationship may be less causal, and more coincident.

[37] 3. The relationship between the seasonal thermocline and Z_{2N} varies geographically. While the thermocline is often assumed to be a proxy for Z_{2N}, this is true only in the tropical regions of Indian and Atlantic oceans. In the subtropical gyres Z_{2N} is deeper than the seasonal thermocline most of the year, but seasonally intercepts the thermocline during winter deepening of the thermocline.

[38] Relationships between CHL and the subsurface fields delineate three geographical regions: the tropics, midlatitudes and high latitudes. The different correlations represent fundamentally different underlying biophysical dynamics: thermocline uplift in the tropics, entrainment in midlatitudes and light limitation at high latitudes. Clearly chlorophyll variability that is associated with grazing pressure, internal ecosystem variability, or physical processes such as atmospheric deposition cannot be accounted for without additional information.

[39] Figure 10 illustrates conceptually the relationships between the physical subsurface dynamics and what we can observe from space; i.e., SSH-TD relationships and CHL-TD relationships, with TD (as a proxy for Z_{2N}) being the mechanistic link between SSH and CHL. Our goal here is to interpret the fields that may be observed remotely with high spatial resolution, i.e., CHL-SSH relationships, as shown in Figure 11, in the context of the underlying processes. Where SSH-TD and CHL-TD correlations are both negative (blue regions in Figure 10), or both positive (dark green in Figure 10), the CHL-SSH relationship should be positive, as is seen in Figure 11 poleward of 40°, in the region of light limitation, and in parts of the tropics. Where the correlation between SSH/TD is negative, and the CHL/TD relationship is positive (medium green regions in Figure 10), the CHL-SSH correlation will be negative, which occurs in the subtropical areas in Figure 11 and represents our entrainment scenario (Figure 6b). Finally, the area where the SSH-TD relationship is positive, but the CHL-TD relationship is negative (pale green regions in Figure 10), yield negative CHL-SSH correlations (Figure 11), and represents the upwelling scenario of Figure 6a. Thus, although Figure 11 is rather complex to interpret, particularly in the tropics, it may be understood mechanistically as a result of the different relationships between SSH-TD and CHL-TD.

[40] This work demonstrates the importance of understanding the regional subsurface dynamics in interpreting the relationships between surface satellite observations. Care is needed in interpreting the relationships between SSH and MLD/TD even within the tropics. However, these relationships may be very useful on interannual timescales for characterizing the changes in these seasonal climatological relationships.

References

Bissett, W. P., M. B. Meyers, J. J. Walsh, and F. E. Müller-Karger (1994), The effects of temporal variability of mixed layer depth on primary productivity around Bermuda, *J. Geophys. Res.*, *99*, 7539–7553.

Carnes, M. R., W. J. Teague, and J. L. Mitchell (1994), Inference of subsurface thermohaline structure from fields measurable by satellite, *J. Atmos. Ocean. Tech.*, *11*, 551–566.

Carr, M. E., O. T. Sato, and P. S. Polito (2004), Interannual variability in new production and nutrient availability (1993–2003) estimated from satellite altimeter: Changes in the North Pacific, *Eos Trans. AGU*, *84*(52), Ocean Sci. Meet. Suppl., Abstract OS31K-05.

Chao, Y., and L.-L. Fu (1995), A comparison between the TOPEX/Poseidon data and a global ocean general circulation model during 1992–1993, *J. Geophys. Res.*, *100*, 24,965–24,976.

Chavez, F. P., P. G. Strutton, and M. J. McPhaden (1998), Biological-physical coupling in the central equatorial Pacific during the onset of the 1997–1998 El Niño, *Geophys. Res. Lett.*, *25*, 3543–3546.

Chu, P. C., C. R. Fralick Jr., S. D. Haeger, and M. J. Carron (1997), A parametric model for the Yellow Sea thermal variability, *J. Geophys. Res.*, *102*, 10,499–10,507.

Chu, P. C., C. Fan, and W. T. Liu (2000), Determination of vertical thermal structure from sea surface temperature, *J. Atmos. Ocean. Technol.*, *17*, 971–979.

Cipollini, P., D. Cromwell, G. D. Quartly, and P. G. Challenor (2000), Remote sensing of oceanic extra-tropical Rossby waves, in *Satellite, Oceanography and Society*, edited by D. Halpern, pp. 99–123, Elsevier, New York.

Coles, V. J., C. Wilson, and R. R. Hood (2004), Remote sensing of new production fueled by nitrogen fixation, *Geophys. Res. Lett.*, *31*, L06301, doi:10.1029/2003GL019018.

Conkright, M. E., et al. (2002), *World Ocean Database 2001,* vol. 1, *Introduction*, 167 pp., NOAA, Silver Spring, Md.

Cronin, M. F., and W. S. Kessler (2002), Seasonal and interannual modulation of mixed layer variability at 0°, 110°W, *Deep Sea Res., Part I*, *49*, 1–17.

Cullen, J. J. (1999), Iron, nitrogen and phosphorus in the ocean, *Nature*, *402*, 372.

de Boyer Montégut, C., G. Madec, A. S. Fischer, A. Lazar, and D. Iudicone (2004), Mixed layer depth over the global ocean: An examination of profile data and a profile-based climatology, *J. Geophys. Res.*, *109*, C12003, doi:10.1029/2004JC002378.

De Mey, P. (1997), Data assimilation at the oceanic mesoscale: A review, *J. Meteorol. Soc. Jpn.*, *75*, 415–427.

Duce, R. A., and N. W. Tindale (1991), Atmospheric transport of iron and its deposition in the ocean, *Limnol. Oceanogr.*, *36*, 1715–1726.

Ferry, N., G. Reverdin, and A. Oschlies (2000), Seasonal sea surface height variability in the North Atlantic Ocean, *J. Geophys. Res.*, *105*, 6307–6326.

Fu, L.-L. (2001), Ocean circulation and variability from satellite altimetry, in *Ocean Circulation and Climate Observing and Modelling the Global Ocean*, edited by G. Siedler, J. Church, and J. Gould, pp. 141–172, Elsevier, New York.

Fukumori, I., R. Raghunath, and L.-L. Fu (1998), Nature of global large-scale sea level variability in relation to atmospheric forcing: A modeling study, *J. Geophys. Res.*, *103*, 5493–5512.

Gardner, W. D., D. J. S. Gundersen, M. J. Richardson, and I. D. Walsh (1999), The role of seasonal and diel changes in mixed-layer depth on carbon and chlorophyll distributions in the Arabian Sea, *Deep Sea Res., Part II*, *46*, 1833–1858.

Garzoli, S. L., and G. J. Goni (2000), Combining altimeter observations and oceanographic data for ocean circulation and climate studies, in *Satellite, Oceanography and Society*, edited by D. Halpern, pp. 79–97, Elsevier, New York.

Gill, A. E., and P. P. Niiler (1973), The theory of seasonal variability in the ocean, *Deep Sea Res.*, *20*, 141–177.

Guinehut, S., P. Y. Le Traon, G. Larnicol, and S. Philipps (2004), Combining Argo and remote-sensing data to estimate the ocean three-dimensional temperature fields—A first approach based on simulated observations, *J. Mar. Syst.*, *46*, 85–98.

Han, G., J. Zhu, and G. Zhou (2004), Salinity estimation using the *T-S* relation in the context of variational data assimilation, *J. Geophys. Res.*, *109*, C03018, doi:10.1029/2003JC001781.

Herbland, A., and B. Voituriez (1979), Hydrological structure analysis for estimating primary production in the tropical Atlantic Ocean, *J. Mar. Res.*, *37*, 87–101.

Houghton, R. W. (1991), The relationship of sea surface temperature to thermocline depth at annual and interannual time scales in the tropical Atlantic Ocean, *J. Geophys. Res.*, *96*, 15,173–15,185.

Ito, T., and M. J. Follows (2003), Upper ocean control on the solubility pump of CO_2, *J. Mar. Res.*, *61*, 465–489.

Jenkins, W. J., and S. C. Doney (2003), The subtropical nutrient spiral, *Global Biogeochem. Cycles*, *17*(4), 1110, doi:10.1029/2003GB002085.

Ji, M., R. W. Reynolds, and D. W. Behringer (2000), Use of TOPEX/Poseidon sea level data for ocean analyses and ENSO predictions: Some early results, *J. Clim.*, *13*, 216–231.

Kara, A. B., P. A. Rochford, and H. E. Hurlburt (2003), Mixed layer depth variability over the global ocean, *J. Geophys. Res.*, *108*(C3), 3079, doi:10.1029/2000JC000736.

Karl, D. M., R. M. Letelier, R. Tupas, J. Dore, J. Christian, and D. V. Hebel (1997), The role of nitrogen fixation in biogeochemical cycling in the subtropical North Pacific Ocean, *Nature*, *388*, 533–538.

Le Quéré, C., L. Bopp, and I. Tegen (2002), Antarctic circumpolar wave impact on marine biology: A natural laboratory for climate change study, *Geophys. Res. Lett.*, *29*(10), 1407, doi:10.1029/2001GL014585.

Letelier, R. M., R. R. Bidigare, D. V. Hebel, M. Ordrusek, C. D. Winn, and D. M. Karl (1993), Temporal variability of phytoplankton community structure based on pigment analysis, *Limnol. Oceanogr.*, *38*, 1420–1437.

Levitus, S., and T. Boyer (1994), *World Ocean Atlas 1994*, vol. 4, *Temperature, NOAA Atlas NESDIS 4*, NOAA, Silver Spring, Md.

Lewis, M. R., W. G. Harrison, N. S. Oakey, D. Herbert, and T. Platt (1986), Vertical nitrate fluxes in the oligotrophic ocean, *Science*, *234*, 870–873.

Longhurst, A. (1995), Seasonal cycles of pelagic production and consumption, *Prog. Oceanogr.*, *36*, 77–167.

Longhurst, A. R. (1998), *Ecological Geography of the Sea*, 398 pp., Elsevier, New York.

Lukas, R., and E. Lindstrom (1991), The mixed layer of the western equatorial Pacific Ocean, *J. Geophys. Res.*, *96*, 3343–3357.

Maes, C. (1999), A note on the vertical scales of temperature and salinity and their signature in dynamic height in the western Pacific Ocean: Implications for data assimilation J, *Geophys. Res.*, *104*, 11,037–11,048.

Martin, J., S. Fitzwater, and R. Gordon (1990), Iron deficiency limits growth in Antarctic waters, *Global Biogeochem. Cycles*, *4*, 5–12.

Mayer, D. A., R. L. Molinari, M. O. Baringer, and G. J. Goni (2001), Transition regions and their role in the relationship between sea surface height and subsurface temperature structure in the Atlantic Ocean, *Geophys. Res. Lett.*, *28*, 3943–3946.

McClain, C. R., S. R. Signorini, and J. R. Christian (2004), Subtropical gyre variability observed by ocean-color satellites, *Deep Sea Res., Part II*, *51*, 281–301.

McGowan, J. A., and T. L. Hayward (1978), Mixing and oceanic productivity, *Deep Sea Res.*, *25*, 771–793.

Nardelli, B. B., and R. Santoleri (2004), Reconstructing synthetic profiles from surface data, *J. Atmos. Ocean. Technol.*, *21*(4), 693–703.

Oschlies, A. (2002), Nutrient supply to the surface waters of the North Atlantic: A model study, *J. Geophys. Res.*, *107*(C5), 3046, doi:10.1029/2000JC000275.

Pingree, R., Y.-H. Kuo, and C. Garcia-Soto (2002), Can the subtropical North Atlantic permanent thermocline be observed from space?, *J. Mar. Biol. Assoc. U.K.*, *82*, 709–728.

Rebert, J. P., J. R. Donguy, G. Eldin, and K. Wyrtki (1985), Relations between sea level, thermocline depth, heat content, and dynamic height in the tropical Pacific Ocean, *J. Geophys. Res.*, *90*, 11,719–11,725.

Reynolds, R. W., N. A. Rayner, T. M. Smith, D. C. Stokes, and W. Wang (2002), An improved in situ and satellite SST analysis for climate, *J. Clim.*, *15*, 1609–1625.

Ryan, J. P., P. S. Polito, P. G. Strutton, and F. P. Chavez (2002), Unusual large-scale phytoplankton blooms in the equatorial Pacific, *Prog. Oceanogr.*, *55*, 263–285.

Sato, O. T., P. S. Polito, and W. T. Liu (2000), Importance of salinity measurements in the heat storage estimation from TOPEX/Poseidon, *Geophys. Res. Lett.*, *27*, 549–551.

Siegel, D. A., D. J. McGillicuddy Jr., and E. Fields (1999), Mesoscale eddies, satellite altimetry and new production in the Sargasso Sea, *J. Geophys. Res.*, *104*, 13,359–13,379.

Sprintall, J., and M. Tomczak (1992), Evidence of the barrier layer in the surface layer of the tropics, *J. Geophys. Res.*, *97*, 7305–7316.

Stammer, D. (1997), Steric and wind-induced changes in TOPEX/Poseidon large scale sea surface topography observations, *J. Geophys. Res.*, *102*, 20,987–21,009.

Tilburg, C. E., B. Subrahmanyam, and J. J. O'Brien (2002), Ocean color variability in the Tasman Sea, *Geophys. Res. Lett.*, *29*(10), 1487, doi:10.1029/2001GL014071.

Turk, D., M. J. McPhaden, A. J. Busalacchi, and M. R. Lewis (2001), Remotely sensed biological production in the equatorial Pacific, *Science*, *293*, 471–474.

Tyrrell, T. (1999), The relative influences of nitrogen and phosphorus on oceanic primary production, *Nature*, *400*, 525–531.

Venrick, E. L. (1993), Phytoplankton seasonality in the central North Pacific: The endless summer reconsidered, *Limnol. Oceanogr.*, *38*, 1135–1149.

Williams, R. G., and M. J. Follows (1998), The ekman transfer of nutrients and maintenance of new production over the North Atlantic, *Deep Sea Res., Part I*, *45*, 461–489.

Wilson, C. (2003), Late summer chlorophyll blooms in the oligotrophic North Pacific subtropical gyre, *Geophys. Res. Lett.*, *30*(18), 1942, doi:10.1029/2003GL017770.

Wilson, C., and D. Adamec (2001), Correlations between surface chlorophyll and sea surface height in the tropical Pacific during the 1997–1999 El Niño–Southern Oscillation event, *J. Geophys. Res.*, *106*, 31,175–31,188.

Wilson, C., and D. Adamec (2002), A global view of bio-physical coupling from SeaWiFS and TOPEX satellite data, 1997–2001, *Geophys. Res. Lett.*, *29*(8), 1257, doi:10.1029/2001GL014063.

————————————

V. J. Coles, University of Maryland Center for Environmental Science, Horn Point Laboratory, P.O. Box 775, Cambridge, MD 21613, USA.

C. Wilson, NOAA/NMFS SWFSC Environmental Research Division, 1352 Lighthouse Ave., Pacific Grove, CA 93950, USA. (cara.wilson@noaa.gov)